

## Technical note

## Fracture resistance of shape memory alloys under thermomechanical loading

J. Makkar <sup>a,1</sup>, B. Young <sup>b,1</sup>, I. Karaman <sup>b</sup>, T. Baxevanis <sup>a,\*</sup><sup>a</sup> Department of Mechanical Engineering, University of Houston, Houston, TX 77204-4006, USA<sup>b</sup> Department of Materials Science and Engineering, Texas A&M University, College Station, TX 77843, USA

## ARTICLE INFO

## Keywords:

Fracture toughness  
Martensitic phase transformation  
Shape memory alloys  
Actuation loading

## ABSTRACT

Experimental measurements of the fracture resistance of Shape Memory Alloys (SMAs) under thermomechanical loading conditions are reported. NiTi compact tension specimens are subjected to either isothermal mechanical or isobaric thermal loading; the latter loading path is an idealization of typical loading paths that utilize these alloys as actuators. A single-parameter description of the experimental data is employed on the basis of a path-independent contour integral, which is approximated by the load-load-line displacement curves recorded from the experiments. The obtained results represent the first experimental measurement of the fracture toughness of SMAs under coupled thermo-mechanical loading, and indicate that the fracture toughness enhancement associated with crack advance under isobaric thermal loading is less pronounced than the corresponding one under isothermal mechanical loading.

## 1. Introduction

Shape Memory Alloys (SMAs) are intermetallics, a relatively brittle class of materials, which fail predominantly by cleavage of specific crystallographic planes [1–5]. However, SMAs do display slow and stable crack extension, *i.e.*, an  $R$ -curve behavior, which is attributed mainly to phase transformation as opposed to plastic deformation in conventional ductile metals. The observed toughening (stable crack growth) is due to irreversibility effects associated with nonproportional straining in the active phase transformation zone and the shielding effect of the transformed material left in the wake of the advancing crack. Stable crack advance has been observed under nominally-isothermal mechanical loading and during cooling under a constant applied load, *i.e.*, under thermomechanical (also termed actuation) loading [6]. Crack advance under the latter loading conditions, which is characteristic to SMAs, is argued to initiate due to transformation occurring in regions in front of the crack tip, resulting in an increase of the crack driving force [7,8].

Phase transformation (and (re)orientation of martensite variants) occurring during the fracture of SMAs call for modifications to the experimental measurement of fracture toughness standards developed for conventional structural metals [9]. Recently, Behrouz et al. [10] proposed a measurement of the  $J_R$ -resistance curve under nominally-isothermal mechanical loading that accounts for the mismatch among the apparent elastic properties of austenite, self-accommodated, and oriented martensite. Further modifications to

\* Corresponding author.

E-mail addresses: [jmakkar@uh.edu](mailto:jmakkar@uh.edu) (J. Makkar), [bey1@tamu.edu](mailto:bey1@tamu.edu) (B. Young), [ikaraman@tamu.edu](mailto:ikaraman@tamu.edu) (I. Karaman), [tbaxevanis@uh.edu](mailto:tbaxevanis@uh.edu) (T. Baxevanis).<sup>1</sup> These authors have contributed equally to this letter.

## Nomenclature

$\Gamma$	cracked configuration's bounding contour
$2\gamma$	energy release at the crack tip per unit crack extension
$\delta$	load-point displacement
$\delta^{el}, \delta^{in}$	elastic and inelastic part of load-point displacement, respectively
$\epsilon_{ij}$	small-strain tensor components
$\eta^{el}, \gamma^{el}$	elastic geometry-dependent factors
$\eta^{in}, \gamma^{in}$	inelastic geometry-dependent factors
$\sigma_{cr}$	critical stress required for initiation of martensitic transformation
$\sigma_{ij}$	stress tensor components
$\sigma_{TS}$	ultimate tensile strength
$\sigma_Y$	effective yield strength
$\rho$	density
$\psi$	Helmholtz free energy
$\Omega$	cracked configuration bounded by contour $\Gamma$
$J^{*el}, J^{*in}$	elastic and inelastic part of $J^*$ , respectively
$A_f$	austenite-finish temperature
$A_s$	austenite-start temperature
$a$	crack length
$B$	CT specimen thickness
$b$	length of the unbroken ligament
$C$	unloading elastic compliance
$H$	heat input
$J, J^*$	path-independent contour integrals
$J_{Ic}^*$	mode-I critical $J^*$
$J_R^*$	resistance $J^*-\Delta a$ curve
$K_{Ic}$	mode-I critical stress intensity factor
$M_f$	martensite-finish temperature
$M_s$	martensite-start temperature
$n_i$	unit vector normal to $\Gamma$ , components of
$P$	imposed force per unit thickness
$q_i$	heat flux vector components
$s$	specific entropy
$T$	absolute temperature
$U$	internal energy
$u$	specific internal energy
$u_i$	displacement vector components
$W$	CT specimen width
$W_\sigma$	density of total stress work
$W_{ext}$	external work done
$A^{el}, A^{in}$	elastic and inelastic area under load-load-line displacement curve, respectively

the ASTM standards regarding the linear compliance method, blunting line slope, and the thickness requirement for  $J$ -dominance may be required for the standardization of fracture toughness testing for SMAs as discussed in [11].

In this technical note, a path-independent contour integral is employed for describing the driving force for crack growth in SMAs under thermomechanical (actuation) loading paths, which collapses to the  $J$ -integral under nominally-isothermal conditions. An approximation of this integral is measured experimentally from the load-load-line displacement curve recorded from experiments on NiTi Compact Tension (CT) specimen during cooling under a constant bias load. The measured  $R$ -curves are presented and compared with those obtained from the same material under nominally-isothermal conditions. The obtained results represent the first experimental measurement of the fracture toughness of SMAs under actuation loading and support the introduction of the employed contour integral as a potential unified descriptor of fracture toughness in SMAs for a wide range of thermomechanical loading conditions (and geometric configurations).

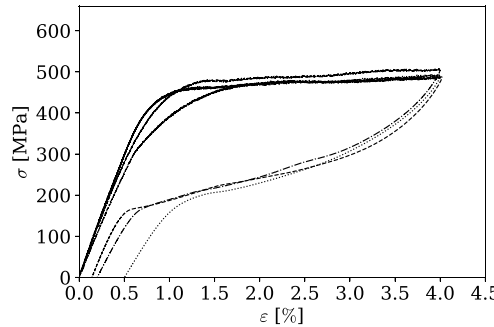


Fig. 1. Uniaxial tensile loading-unloading stress-strain curves for 3 experiments performed on Ni<sub>55.7</sub>Ti (wt%) at room temperature.

## 2. Material, methodology, and results

Fracture toughness tests were performed on Ni<sub>55.7</sub>Ti<sub>44.3</sub> (wt%) Compact Tension (CT) specimens in an MTS-810 servo-hydraulic test frame. The phase transition temperatures of the alloy, which was acquired from Fort Wayne Metals and is superelastic at room temperature (Fig. 1), are  $M_f = -29^\circ\text{C}$ ,  $M_s = -20^\circ\text{C}$ ,  $A_s = -15^\circ\text{C}$  and  $A_f = 7^\circ\text{C}$ , where  $M_f$ ,  $M_s$ ,  $A_s$  and  $A_f$  indicate martensite finish, martensite start, austenite start and austenite finish temperatures, respectively, determined using a TA Instruments Q2000 Differential Scanning Calorimetry (DSC). The dimensions of the specimen (schematic in Fig. 2a) were  $W \approx 32.5$ ,  $B \approx 8.5$ ,  $0.45 \leq a/W \leq 0.55$ , all in mm, where  $a$  is the crack size. The samples were cut from the bulk using wire Electrical Discharge Machining (EDM), and both sides were metallographically prepared by mechanical grinding using abrasive papers to remove the EDM recast layer and for a better surface finish for optical crack size measurements. The specimens were fatigue pre-cracked in load control with load values between 0.1 and  $P_{max}$  at a frequency of 10 Hz, where  $P_{max}$ , initially set equal to 20% of the highest load value measured in the fracture experiments, was gradually decreased. During pre-cracking, the crack size was optically monitored from both sides of the specimen until the desired initial crack size ( $a_0$ ) was obtained. The isothermal tests were performed in displacement control at a loading rate of 0.09 mm/min. The isobaric fracture tests were conducted by inductively heating the CT specimen to 100 °C to ensure complete transformation to austenite, increasing the load to one that corresponds to 95% of isothermal  $K_{Ic}$  to ensure small-scale transformation conditions at initiation of crack growth, and then cooling down at a rate of 1 °C /min to room temperature. This cooling rate was chosen to allow (i) for a homogeneous temperature throughout the sample (being slow enough), as measured using the thermocouples, and (ii) for an unloading/reloading cycle to take place in order to measure the specimen compliance at specific temperatures. Crack extension was measured by the elastic compliance method [12,13], in accordance with the ASTM standards [9]. The compliance was measured by partial unloads and reloads, which were performed by decreasing the displacement by 0.05 mm at 0.15 mm intervals in the case of isothermal tests and by decreasing the load to 80% of the maximum load while keeping the temperature constant in the case of the isobaric tests. Load and load-line displacement (LLD) were continuously measured at a rate of 10 Hz throughout the tests using an Interface 2500 kN load cell and clip-on crack tip opening displacement extensometer by Epsilon Technology Corp. Optical images were recorded at rates of 2 fps (isothermal tests) and 0.1 fps (isobaric tests) on one side of the CT specimens, which was speckled to produce a random pattern, using a Point Grey Blackfly CCD camera equipped with Canon 18–55 mm lens at an optical resolution of 0.02 mm/pixel and were post-processed via Vic2D-6 software (developed by Correlated Solutions) to measure the full-field Lagrangian strain using Digital Image Correlation (DIC) [14].

The experimental load-load-line displacement curves are shown in Figs. 2. In the isothermal tests, the response is initially linear, characterized almost entirely by elastic deformation, followed by a nonlinearity associated with increasing phase transformation close to the crack tip, crack advance and resulting reorientation of martensite variants, and to a lesser extent plastic deformation [4]. The monotonicity of the applied load is interrupted by a sequence of partial unloading/reloading cycles performed in order to measure the CT specimen compliance and in turn the crack advance. The load-load-line displacement curves for the isobaric experiments are mostly linear during the application of the mechanical load at 100 °C. During the subsequent cooling while the bias load is kept constant, the load-line displacement increases as the phase transformation zone expands close to the crack tip, where the stresses are high, due to the Clapeyron slope, interrupted periodically by partial unloads/reloads. Reorientation of martensite variants is expected in the wake of the growing crack.

The experimental measurement of the path-independent contour integral  $J^*$ , introduced in Appendix, can be based on its energetic definition

$$J^* = -\frac{d}{da} \left( \int_{\Omega} W_{\sigma} dV + \int_{\Gamma} n_i \sigma_{ij} u_j dS \right), \quad (1)$$

derived from (A.2) and (A.6). Under the assumption of fixed displacements (grips), the second term in the above equation vanishes, and  $J^*$  can be approximated as

$$J^* \approx \int_0^{\delta} \left( \frac{\partial P}{\partial a} \right)_{\delta} d\delta, \quad (2)$$

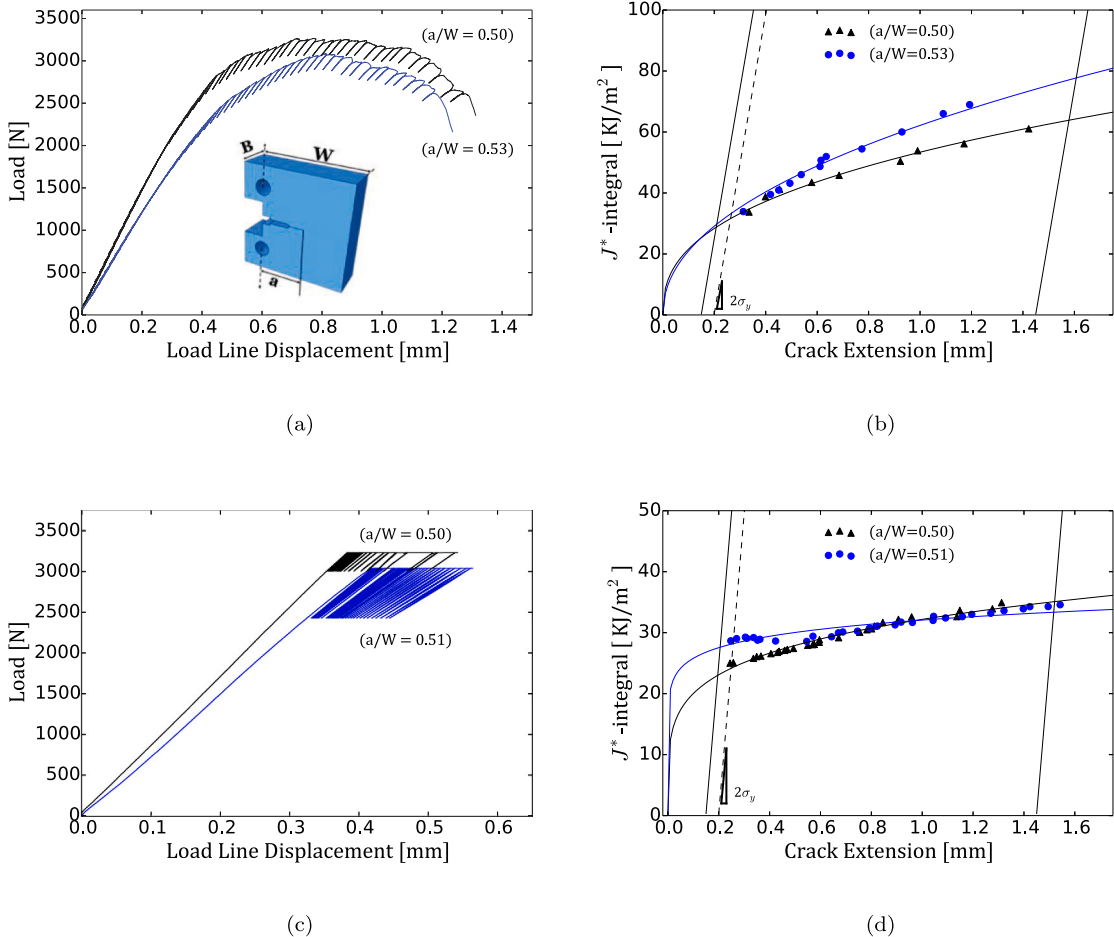


**Fig. 2.** load-load-line displacement (LLD) and  $J_R^*$ -curves for the isobaric and isothermal fracture tests. In all experiments  $0.45 < a/W < 0.55$ , and  $3.95 < B < 4.05$  mm. (a) & (b) isothermal experiments and (c) & (d) isobaric experiments.

**Table 1**  
 $J_{I_c}^*$ -values [ $\text{KJ/m}^2$ ] for  $\text{Ni}_{55.7}\text{Ti}_{44.3}$  (wt%) SMA determined by the method of offset line from isothermal and isobaric fracture experiments with unloading-reloading steps to determine the system compliance.

Experiment	Isothermal		Isobaric	
	A	B	C	D
$J_{I_c}^*$ -value [ $\text{KJ/m}^2$ ]	31.9	30.3	27.8	24.6

where  $P$  is the imposed force per unit thickness and  $\delta$  is the load point displacement [15].

The  $J^*$ -value can therefore be measured from the load-load-line displacement record of the CT specimens by correlating  $J^*$  and the work of deformation  $\int_0^\delta P d\delta$ , i.e., the area under the load-displacement curve [16–18], as  $J^* = J^{*el} + J^{*in} = \frac{\eta^{el} A^{el}}{Bb} + \frac{\eta^{in} A^{in}}{Bb}$ , where  $b = W - a$  is the length of the unbroken ligament.  $A^{el}$  and  $A^{in}$  are the elastic and inelastic components of the area under the load-load-line displacement curve, respectively.  $\eta^{el}$  and  $\eta^{in}$  are geometry-dependent factors, the existence of which is discussed in [10,11]. The expression for the  $J^*$ -integral given above is valid only for constant crack length,  $a$ . For advancing cracks, an incremental formulation is needed [19],  $J_i^* = J_i^{*el} + J_i^{*in}$ , where  $J_i^{*el}$  and  $J_i^{*in}$  are evaluated from the previous step  $J_i^\alpha = \left[ J_{i-1}^\alpha + \frac{\eta_{i-1}^\alpha}{Bb_{i-1}} A_{i-1,i}^\alpha \right] \left[ 1 - \frac{\gamma_{i-1}^\alpha}{b_{i-1}} (a_i - a_{i-1}) \right]$ . In the last equation, the superscript  $\alpha$  stands for either  $^{el}$  or  $^{in}$ ,  $A_{i-1,i}^{el}$  and  $A_{i-1,i}^{in}$  are the increments of the elastic and inelastic areas under the load-load-line displacement record from step  $i - 1$  to  $i$ , respectively,  $A_{i-1,i}^\alpha = \frac{1}{2}(P_i + P_{i-1})(\delta_i^\alpha - \delta_{i-1}^\alpha)$ , where  $\delta_i^{el} = P_i C_i$  and  $\delta_i^{in} = \delta_i - \delta_i^{el}$  are the elastic and inelastic components of the displacement, and  $C_i$  is the unloading elastic compliance.  $\gamma^{el}$  and  $\gamma^{in}$  are geometry-dependent factors and can be determined using  $\eta^{el}$  and  $\eta^{in}$ , respectively [10,11].

Once  $J^*$  and  $\Delta a$  values are known, as outlined above and detailed in [10,11], the  $J_R^*$ -curves are constructed according to the ASTM standards (Fig. 2). A construction line is plotted from the origin of  $J^*$  vs  $\Delta a$  plot with a slope of  $2\sigma_Y$ , where  $\sigma_Y$  is the effective yield

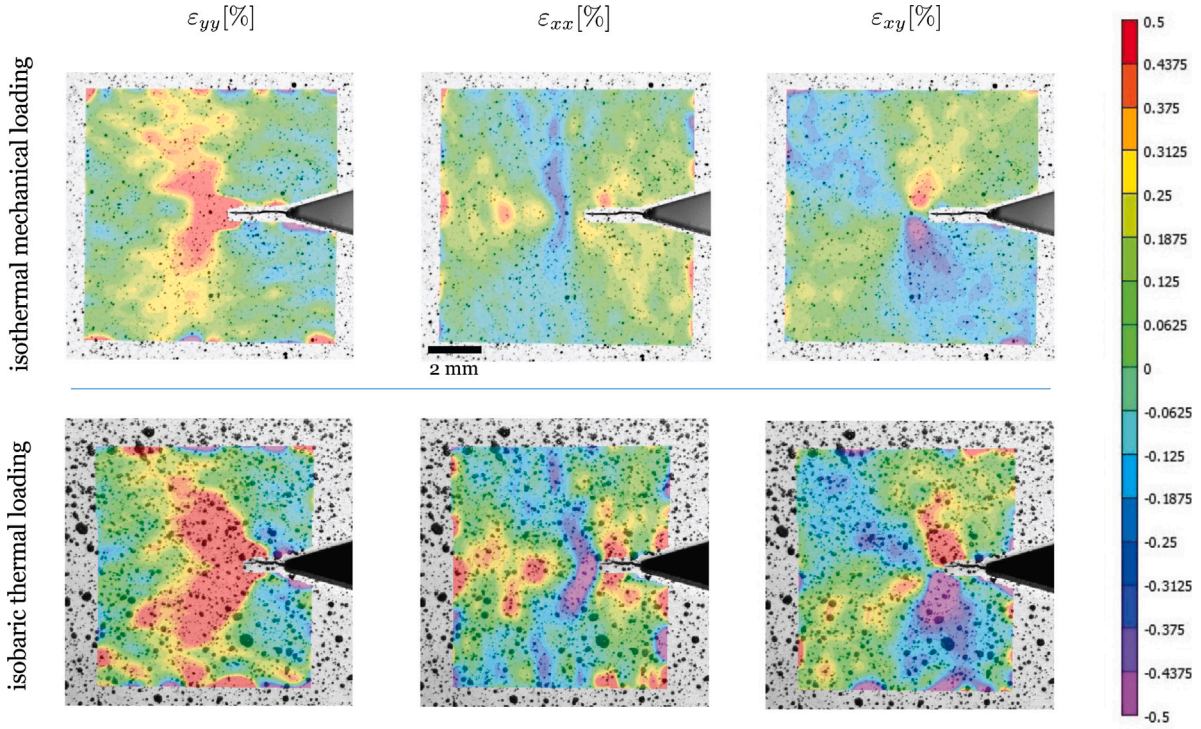


**Fig. 3.** Surface strain contour plots obtained from *in situ* DIC on the Ni<sub>55.7</sub>Ti<sub>44.3</sub> (wt%) CT specimens under two different thermomechanical loading paths. The y-axis is in the direction of loading. Note that the strain values at given distances from the crack tip are larger for the isobaric thermal loading although the crack length is smaller.

strength, *i.e.*, the average of the critical stress,  $\sigma_{cr}$ , required for initiation of phase transformation and the ultimate tensile strength,  $\sigma_{TS}$ . The  $J^* \Delta a$  data points that fall between two exclusion lines, which are drawn parallel to the construction line intersecting the abscissa at 0.15 mm and 1.5 mm, are plotted and a power-law regression is fit throughout. To determine the  $J_{I_C}^*$  fracture toughness, an offset line is then plotted parallel to the construction line, intersecting the abscissa at 0.2 mm. The intersection of the 0.2 mm offset line and the regression line defines an interim value of the  $J$ -integral. This interim value is considered a conservative, constraint-independent fracture toughness value if the qualification requirement of ASTM standards [9],  $B > 10 J_{I_C}^* / \sigma_Y$ , related to the specimen thickness is met.

The following observations can be made.

- The critical  $J_{I_C}^*$ -values measured using the 0.2 mm offset approach from all experiments are close to each other (Table 1). The ~10%–15% difference among the critical values measured should be attributed to the following factors: (i) The quasi-brittle transgranular (quasi-cleavage) fracture and pronounced material variability in the deformation response of SMAs (Fig. 1) result in a pronounced failure response variability; (ii) The default slope,  $2\sigma_Y$ , of the offset line approximates the apparent crack advance due to crack-tip blunting when there is no slow stable crack tearing. This approximation assumes that, before tearing, the crack advance is equal to one half of the crack-tip opening displacement under nominally-isothermal mechanical loading. However, crack-tip blunting in SMAs is path-dependent [20] and, thus, such a slope should assume different values for the two loading conditions (isothermal vs isobaric).
- The proximity of the critical values obtained corroborates that the path-independent  $J^*$ -integral can capture enough of the correct physics to describe with sufficient accuracy the driving force for crack advance in SMAs under both tested conditions. Due to the theoretical arguments resulting in its definition (further discussed below), the  $J^*$ -integral may be adopted as an engineering tool for fracture of SMAs under a wide range of thermomechanical loading conditions and crack configurations. It should be noted that the proximity in the  $J_{I_C}^*$ -values is attained while the intensity of the strain field under isothermal mechanical loading is lower than the corresponding one during isobaric thermal loading (their spatial distribution being similar), which leads to the inverse conclusion regarding the intensity of stress fields (Fig. 3). In the former case, crack growth is driven by the increasing load-line displacement, which results in bias load changes at the loading pins and stress-induced martensite close to the crack tip. In the latter case, crack growth is driven by temperature changes, which result in increasing load-line displacement due to the induced phase transformation close to the crack tip while the bias load at the loading pins is kept constant.
- The slope of the isothermal  $J_R^*$ -curves is steeper than that of the isobaric ones, which indicates that the toughness enhancement associated with crack advance in the experiments under the isothermal conditions is more pronounced than the corresponding

one in the experiments under the isobaric conditions. The consensus is that the toughness enhancement associated with crack advance is attributed to irreversibility effects associated with nonproportional straining in the active inelastic zone and the irrecoverable deformation left in the wake of the growing crack [21–26]. Unfortunately, it is not clear from the DIC results alone how these two stabilizing mechanisms are affected by the thermomechanical loading paths considered; numerical simulations may contribute towards the required insight. Our current assumption is that the “deterministic” toughness enhancement associated with crack advance under isothermal conditions should be independent of temperature in the temperature range that ensures a  $J^*$ -controlled crack growth (as experimentally indicated in [10] for temperatures at which the crack grows in martensite), similarly independent of load under isobaric conditions, and that these conditions are limiting cases of the general thermomechanical conditions.

Given its definition, the  $J^*$ -integral should be further applicable for thermomechanical loading paths for which the deformation response of SMAs can be approximated by a potential  $\psi(\epsilon_{ij}, T)$  such that for a given loading path there is an “1–1” correspondence between the stress  $\sigma_{ij} = \rho \frac{\partial \psi}{\partial \epsilon_{ij}}$  and strain  $\epsilon_{ij}$ ; such an approximation is expected to be valid for a wide range of thermomechanical loading paths involving nearly proportional mechanical loading and monotonic temperature changes.

### 3. Conclusions

A one-parameter interpretation of the experimental data from fracture experiments on SMAs under coupled thermo-mechanical loading is reported. The interpretation of the data is based on an approximation of the value of a path-independent contour integral by the load–load line displacement record measured. The obtained results, which represent the first experimental measurement of the fracture toughness of SMAs under actuation loading conditions, suggest that (i) the employed contour integral should achieve similitude for a wide range of thermomechanical loading conditions and geometric configurations, and that (ii) isothermal conditions provide a more pronounced toughness enhancement as compared to thermal loading under a constant bias load.

### Declaration of competing interest

The authors declare that they have no known competing financial interests or personal relationships that could have appeared to influence the work reported in this paper.

### Acknowledgments

This study was supported by the US Air Force Office of Scientific Research under Grant No. FA9550-18-1-0276, the National Science Foundation under Grants no. CMMI-1917441 and CMMI-1917367, and by NASA-ULI under Grant No. NNX17AJ96A.

### Appendix. A path-independent contour integral for the one-parameter description of fracture toughness in SMAs under thermomechanical loading

For introducing a path-independent contour integral that can achieve similitude over a wide range of loading conditions and geometric configurations, the SMA deformation response is approximated by a thermo-hyperelastic material law with a Helmholtz free energy of the form

$$\psi(\epsilon_{ij}, T) \equiv u[\epsilon_{ij}, s(\epsilon_{ij}, T)] - Ts(\epsilon_{ij}, T), \quad (\text{A.1})$$

where  $u$  is the specific internal energy,  $s = -\frac{\partial \psi}{\partial T}$  is the specific entropy,  $T = \frac{\partial u}{\partial s}$  is the absolute temperature, and  $\epsilon_{ij}$  are the components of the small strain tensor.

Assuming quasi-static loading, the energy release at the crack tip per unit crack extension,  $2\gamma$ , is given from global energy considerations as [27,28]

$$2\gamma\dot{a} + \frac{dU}{dt} = \frac{dW_{ext}}{dt} + \frac{dH}{dt}, \quad (\text{A.2})$$

where  $U$  is the internal energy,  $W_{ext}$  is the external work done,  $H$  is the heat input, and  $\dot{a} > 0$  is the crack velocity. Assuming plane strain conditions, ignoring body forces and heat sources/sinks, and taking into account the Legendre transformation (A.1) and the definition of the small strain tensor, the above energy balance can be written

$$2\gamma\dot{a} + \frac{d}{dt} \left( \int_{\Omega} \rho\psi \, dV \right) = \int_{\Gamma} n_i \sigma_{ij} \frac{\partial u_j}{\partial t} \, dS - \frac{d}{dt} \left( \int_{\Omega} q_i T s \, dV \right) - \int_{\Gamma} q_i n_i \, dS, \quad (\text{A.3})$$

where  $\Omega$  is the cracked configuration, bounded by contour  $\Gamma$ ,  $\rho$  is the density,  $\sigma_{ij}$  are the components of the stress tensor,  $q_i$  are the components of the heat flux vector,  $n_i$  those of the unit vector normal to the  $\Gamma$ , and  $u_i$  are the components of the displacement vector. Assuming that the displacement and temperature distributions move rigidly with the crack tip in the region  $\Omega$ , the temperature is bounded at the crack tip, and the crack grows in the  $x_1$ -direction, the following relations hold true [27]

$$\frac{\partial u_j}{\partial t} = -\dot{a} \frac{\partial u_j}{\partial x_1}, \quad \frac{\partial T_j}{\partial t} = -\dot{a} \frac{\partial T_j}{\partial x_1}, \quad \frac{d}{dt} \left( \int_{\Omega} \rho\psi \, dV \right) = -\dot{a} \int_{\Gamma} n_i \rho\psi \, dS, \quad (\text{A.4})$$

$$\int_{\Gamma} q_i n_i dS = \int_{\Omega} \frac{\partial q_i}{\partial x_i} dV = \int_{\Omega} \rho s \frac{\partial T}{\partial t} dV - \frac{d}{dt} \left( \int_{\Omega} \rho T s dV \right). \quad (\text{A.5})$$

For the derivation of the last equation,

$$\frac{dU}{dt} = \frac{dW}{dt} + \frac{dH}{dt}, \quad (\text{A.6})$$

which holds for every thermomechanical process, and (A.1) were taken into account, where  $W_{\sigma} = \int_0^{\varepsilon_{ij}} \sigma(\varepsilon_{ij}, T) d\varepsilon_{ij}$  is density of total stress work. Given (A.4) and (A.5), the energy balance equation (A.3) takes the form

$$J^* = \int_{\Gamma} \left( \psi dx_2 - \sigma_{ij} \frac{\partial u_j}{\partial x_1} ds \right) + \int_{\Omega} s \frac{\partial T}{\partial x_1} dA = 2\gamma. \quad (\text{A.7})$$

To prove the path-independence of  $J^*$ , it suffices to show that  $J^* \equiv 0$  when integrated over any defect-free region  $\Omega^*$ , bounded by contour  $\Gamma^*$ . To this end, note that the differential of the equation of state (A.1) asserts that

$$\frac{\partial \psi}{\partial x_k} = \frac{1}{\rho} \sigma_{ij} \frac{\partial}{\partial x_i} \left( \frac{\partial u_j}{\partial x_k} \right) - s \frac{\partial T}{\partial x_k} \stackrel{\frac{\partial \sigma_{ij}}{\partial x_i} = 0}{\Rightarrow} \frac{\partial}{\partial x_i} \left( \rho \psi \delta_{ik} - \sigma_{ij} \frac{\partial u_j}{\partial x_k} \right) + \rho s \frac{\partial T}{\partial x_k} = 0. \quad (\text{A.8})$$

Assuming plane strain conditions, integration of the above equation results in

$$\int_{\Gamma^*} n_i \left( \psi \delta_{ik} - \sigma_{ij} \frac{\partial u_j}{\partial x_k} \right) ds + \int_{\Omega^*} s \frac{\partial T}{\partial x_k} dA = 0, \quad (\text{A.9})$$

and, thus, for  $k = 1$ ,  $J^* = 0$ .

## References

- [1] Baxevanis T, Lagoudas DC. Fracture mechanics of shape memory alloys: Review and perspectives. *Int J Fract* 2015;191(1-2):191–213.
- [2] Robertson SW, Pelton AR, Ritchie RO. Mechanical fatigue and fracture of Nitinol. *Int Mater Rev* 2012;57(1):1–37.
- [3] Gollerthan S, Young ML, Baruj A, Frenzel J, Schmahl WW, Eggeler G. Fracture mechanics and microstructure in NiTi shape memory alloys. *Acta Mater* 2009;57(4):1015–25.
- [4] Ungár T, Frenzel J, Gollerthan S, Ribárik G, Balogh L, Eggeler G. On the competition between the stress-induced formation of martensite and dislocation plasticity during crack propagation in pseudoelastic NiTi shape memory alloys. *J Mater Res* 2017;32(23):1–10.
- [5] Makkar J, Baxevanis T. On the fracture response of shape memory alloys by void growth and coalescence. *Mech Mater* 2021;153:103682.
- [6] Jape S, Young B, Haghgouyan B, Hayrettin C, Baxevanis T, Lagoudas DC, et al. Actuation-induced stable crack growth in near-equiautomatic nickel-titanium shape memory alloys: Experimental and numerical analysis. *Int J Solids Struct* 2020. <http://dx.doi.org/10.1016/j.ijsolstr.2020.09.032>.
- [7] Baxevanis T, Parrinello AF, Lagoudas DC. On the driving force for crack growth during thermal actuation of shape memory alloys. *J Mech Phys Solids* 2016;89:255–71.
- [8] Jape S, Baxevanis T, Lagoudas DC. Stable crack growth during thermal actuation of shape memory alloys. *Shape Memory Superelast* 2016;2:104–13.
- [9] ASTM-E1820. Standard test method for measurement of fracture toughness. Technical report, ASTM International, West Conshohocken, PA; 2016.
- [10] Haghgouyan B, Hayrettin C, Baxevanis T, Karaman I, Lagoudas DC. Fracture toughness of NiTi: Towards establishing standard test methods for phase transforming materials. *Acta Mater* 2019;162:226–38.
- [11] Makkar J, Baxevanis T. Notes on the experimental measurement of fracture toughness of shape memory alloys. *J Intell Mater Syst Struct* 2020;31(3):475–83.
- [12] Clarke GA, Andrews WR, Paris PC, Schmidt DW. Single specimen tests for  $J_{Ic}$  determination. In: Mechanics of crack growth. ASTM International; 1976.
- [13] Joyce JA, Gudas JP. Computer interactive  $J_{Ic}$  of testing navy alloys. In: Elastic-plastic fracture. ASTM International; 1979.
- [14] Schreier H, Orteu JJ, Sutton MA. Image correlation for shape, motion and deformation measurements. Springer US; 2009.
- [15] Rice JR. A path independent integral and the approximate analysis of strain concentration by notches and cracks. *J Appl Mech* 1968;35(2):379–86.
- [16] Ernst H, Paris PC, Rossow M, Hutchinson JW. Analysis of load-displacement relationship to determine JR curve and tearing instability material properties. In: Fracture mechanics: proceedings of the eleventh national symposium on fracture mechanics: Part I. ASTM International; 1979.
- [17] Merkle JG, Corten HT.  $J$  integral analysis for the compact specimen, considering axial force as well as bending effects. Technical report, Oak Ridge National Lab., Tenn.(USA); Illinois Univ., Urbana (USA). Dept. of Theoretical and Applied Mechanics; 1973.
- [18] Clarke GA, Landes JD. Evaluation of the  $J$  integral for the compact specimen. *J Test Eval* 1979;7(5):264–9.
- [19] Ernst HA, Paris PC, Landes JD. Estimations on  $J$  integral and tearing modulus T from a single specimen test record. In: Fracture mechanics. ASTM International; 1981.
- [20] Baxevanis T, Lagoudas DC. A mode I fracture analysis of a center-cracked infinite shape memory alloy plate under plane stress. *Int J Fract* 2012;175:1–16.
- [21] Hutchinson JW. On steady quasi-static crack growth. Technical report DEAP S-8, Division of Applied Sciences, Harvard University; 1974.
- [22] Rice JR. Elastic-plastic models for stable crack growth. In: Mechanics and mechanisms of crack growth (Proc. 1973). 1975. p. 14–39.
- [23] Drugan WJ, Rice JR, Sham TL. Asymptotic analysis of growing plane strain tensile cracks in elastic-ideally plastic solids. *J Mech Phys Solids* 1982;30(6):447–73.
- [24] Rice JR, McMeeking RM, Parks DM, Sorensen EP. Recent finite element studies in plasticity and fracture mechanics. *Comput Methods Appl Mech Engrg* 1979;17-18:411–42.
- [25] Dean RH, Hutchinson JW. Quasi-static steady crack growth in small scale yielding. In: Fracture mechanics. ASTM-SP 700, 1980, p. 383–405.
- [26] Makkar J, Young B, Karaman I, Baxevanis T. Experimental observations of “reversible” transformation toughening. *Scr Mater* 2021;191:81–5.
- [27] McCartney LN. Discussion: “The use of the J-integral in thermal stress crack problems”. *Int J Fract* 1979;15(6):R217–21.
- [28] Atluri SN. Energetic approaches and path-independent integrals in fracture mechanics. In: Atluri SN, editor. Computational methods in the mechanics of fracture. Amsterdam: North-Holland; 1986. p. 121–65.